Miranda-Domínguez, O., Feczko, E., Grayson, D. S., Walum, H., Nigg, J. T., & Fair, D. A. (2017). Supplemental Data Items for "Heritability of the human connectome: a connectotyping study." *Network Neuroscience, 2*(2), 175-199. https://doi.org/10.1162/netn_a_00029

Heritability of the human connectome: a connectotyping study

Supplemental data items

Supplemental Results

In this section we report the findings obtained after characterized brain connectivity using Pearson's correlation and performing the same experiments done in the main manuscript.

Comparing consistency within individuals, between siblings, and across unrelated pairs using traditional functional connectivity matrices.

To assess the traditional pearson correlation-based FC approach, we compared how similar the connectivity matrices were between groups (Same individual, predicting data in a different scan session; Individual predicting a sibling; individual predicting an unrelated participant). Here instead of using the model to "predict timecourses" we simply calculated the spatial correlation coefficient between matrices (see Supplemental Methods for details) ending up again with as many correlations as ROIs for each scan-pair being compared. These spatial correlations were then averaged providing 1 mean correlation value for each paired comparison. The distributions of mean average spatial correlations across all pairs are shown in Figure 1-Figure Supplement 4 panel c (*Note: we also compared spatial correlations for the beta weights or connectotypes* and present the corresponding distributions in Figure 1-Figure Supplement 4 panel b). Then, we used a t-test to compare distributions for siblings and unrelated participants. Spatial correlations for both connectotyping and traditional correlations showed that sibling pairs were significantly more similar than unrelated pairs ($p < 1.23\times10^{-6}$ for connectotyping (Figure 1 − Figure Supplement 2b) and $p < 8.96\times10^{-3}$ for correlations (Figure 1 − Figure Supplement 2c).

Classification of simply pairs in youth utilizing traditional function connectivity matrices.

For traditional functional connectivity correlations, the average out-of-sample accuracy was 69%. This finding was significantly higher than null, $p < 10^{-6}$). Sensitivity was 68% and a specificity was 69%. The classifications were mainly driven by ROIs belonging to the following functional networks: cingulo-opercular, dorsal attention, default mode, and ventral attention (Figure 3-Figure Supplement 5, panels D-E). As above, we did not observe significant changes in accuracy when a different number of features were used for classification (Figure 3-Figure Supplement 6 panel A).

Classification of sibling pairs in adults using Human Connectome Project data using traditional correlations

Classification by traditional functional connectivity correlations rendered significant out-of-sample classification accuracies, as shown in Figures 4-Figure Supplement 3 and Figure 4-Figure Supplement 4 (difference in accuracy for identical versus non-identical twins was also significant: $p < 10^{-6}$ rank-sum test, cohen's d = 4.07). Overall, these results suggest that kinship substantially contributes to individualized patterns of complex brain organization. Furthermore, greater accuracy for predicting monozygotic vs dizygotic twins strongly suggests that these patterns are partially heritable.

Classification of sibling pairs using independent datasets

Our validation approach using one dataset to predict siblings vs unrelated was repeated using correlations. As shown in Figure 5-Figure Supplement 2, the overall accuracy with traditional correlations was low (56%, $p < 10^{-6}$ rank-sum test, cohen's d = 2.07).

Quantifying the heritability of the human connectome

Heritability was also quantified for correlation measures using three-way (shared environment X shared genetics X ROI) repeated measures ANOVAs, with ROI as the repeated measure. Heritability estimates (shared genetics) were made at the level of each of the 352 individual regions (333 cortical + 19 subcortical), each of the 14 networks, the whole brain, and for all individual ROI-ROI correlations (Figure 7-Figure Supplement 3).

Correlations showed significant heritability for 283 of the 352 individual ROIs ($h^2 < 0.05$, $p < 0.05$ corrected for multiple comparisons). Figure 7-Figure Supplement 2 plots the heritability of the top 100 features of the SVM for correlations. Heritability is also low at the level of individual regions.

Therefore, we examined the heritability across the whole brain and for each network for traditional functional connectivity correlations, controlling for the effect of individual ROIs via repeated-measures ANOVA. For correlations (Figure 7-Figure Supplement 2A, top; $h^2 > 0.49$, $p < 1e\text{-}6$) dorsal attention and frontal parietal systems were among the most heritable, paralleling the most used networks for SVM. Thus, the SVM is likely capturing some heritability of individual networks. Across the whole brain, heritability was much greater ($h^2 = 0.53$ (upper 95% CI = 0.57, lower 95% CI = 0.48; $p < 1e\text{-}6$) than at the level of individual regions or networks and further suggests that rather than individual connections, groups of functional connections are heritable

Using the same repeated measures ANOVA we found that the shared environment of networks was greater for the whole brain than for individual connections (Figure 7-Figure Supplement 3). However, these results are difficult to interpret because no-twin sibling pairs represent a large

portion of our data, so we are reluctant to interpret these results with too much emphasis. A twin design with greater numbers than presented here would be required to properly estimate shared environment.

For traditional correlations, no individual connection showed statistically significant heritability after correction for multiple comparisons. Nevertheless, we quantified heritability and environment from the generalized linear mixed model for the top 100 features used in SVM, which showed little variation in heritability (Figure 7-Figure Supplement 3, black circle) or shared environment (Figure 7-Figure Supplement 3; black plus sign).

Spatial correlations show significant heritability and shared environment in both the 198 (heritability: Figure 7-Figure Supplement 2; shared environment: Figure 7-Figure Supplement 3, red plus sign) and 499 (heritability: Figure 7-Figure Supplement 3, blue circle; shared environment: Figure 7-Figure Supplement 3, blue plus sign) datasets. Taken together, the set of results suggests that connections between groups but not pairs of brain regions may be heritable.

Motion familiality:

Because a prior study reported that the degree of motion in resting-state data may be heritable, we used a general linear mixed model to evaluate familiality in the OHSU dataset. As above, the "fitlmematrix" function in matlab was used to construct and test the generalized linear mixed model. Because the OHSU dataset contained no twins, we could not dissociate shared environmental from shared genetic effects. Therefore, the familiality matrix represents the familiality between subjects; sibling pairs have a correlation of 1 and non-sibling pairs have a correlation of 0. The eigenvalues derived from the familiality matrix were used as the random factor, with sex and age as covariates. Point estimates of familiality were calculated by

measuring the ratio of the familiality component to the total variance. Pre-censored and post-censored OHSU datasets were tested for motion familiality.

Supplemental Methods

MRI Data Acquisition:

Oregon: Structural images were obtained using a T1-weighted MP-RAGE sequence (TR=2.3s, TE=3.58ms, flip angle = 10°, TI = 900ms, voxel size = 1mm^3, 160 sagittal slices). A T2-weighted sequences was also acquired (TR = 3.2s, TE = 497ms, voxel size = 1mm, slices = 160) as well as magnitude and phase field maps to correct for geometric distortions due to susceptibility artifact. Resting-state functional BOLD images were acquired using a gradient-echo, echo-planar sequence (TR = 2500 ms, TE = 30 ms; FOV = 240 mm; flip angle = 90°; 3.75x3.75x3.8 mm). Full brain coverage was obtained with 36 contiguous interleaved 3.8 mm axial slices acquired parallel to the plane transecting the anterior and posterior commissure.

HCP: We note that HCP data was acquired on a 3T Siemens Skyra optimized to achieve 100 mT/m gradient strength. All the data was corrected to account for the non-linearities associated with the high gradient and the displacement of the isocenter in this optimized system. For further details see the HCP 500 Subjects + MEG2 Data Release: Reference Manual (WU-Minn, 2014) and (Glasser et al., 2013).

Two separate T1-weighted images were acquired and averaged, with a TR=2400 ms, TE=2.14 ms, TI = 1000 ms, FA = 8°, and ES = 7.6 ms. Two T2-weighted images were acquired and averaged with a TR=3200 ms, TE=565 ms. T1-weighted and T2-weighted images were acquired with a voxel resolution of 0.7 mm (isotropic). Resting state BOLD data were acquired using a gradient echo echo planar imaging sequences with 2mm^3 voxels, TR=720ms, TE = 33.1ms, and a multiband acceleration factor of 8.

MRI Data Preprocessing:

Oregon: Data were processed using the pipelines from the Human Connectome Project (Glasser et al. 2013), which include the use of FSL (Smith et al. 2004; Jenkinson et al. 2012; Woolrich et al. 2009) and FreeSurfer tools (Dale et al. 1999; Desikan et al. 2006; Fischl & Dale 2000). Briefly, gradient distortion corrected T1-weighted and T2-weighted volumes were first aligned to the MNI's AC-PC axis and then non-linearly normalized to the MNI atlas. Later, the T1w and T2w volumes are re-registered using boundary based registration (Greve & Fischl 2009) to improve alignment. Then, the brain is segmented using recon-all from FreeSurfer. Segmentations are improved by using the enhanced white matter-pial surface contrast of the T2-weighted sequence. The BOLD data is corrected for field distortions (using FSL's TOPUP) and processed by doing a preliminary 6 degrees of freedom linear registration to the first frame. After this initial alignment, the average frame is calculated and used as final reference. Next, the BOLD data is registered to this final reference and to the T1-weighted volume, all in one single step, by concatenating all the individual registrations into a single registration.

Surface registration. The cortical ribbon defined by the structural T1-weighted and T2-weighted volumes is used to define a high resolution mesh which will be used for surface registration of the BOLD data. This cortical ribbon is also used to quantify the partial contribution of each voxel in the BOLD data in surface registration. Timecourses in the cortical mesh are calculated by obtaining the weighted average of the voxels neighboring each vertex within the grid, where the weights are given by the average number of voxels wholly or partially within the cortical ribbon. Voxels with high coefficient of variation, indicating difficulty with tissue assignment or containing large blood vessels, are excluded. Next, the resulting timecourses in this mesh are

downsampled into a standard space of anchor points (grayordinates), which were defined in the brain atlas and mapped uniquely to each participant's brain after smoothing them with a 2mm full-width-half-max Gaussian filter. Subcortical regions are treated and registered as volumes. Two thirds of the grayordinates are vertices located in the cortical ribbon while the remaining grayordinates are subcortical voxels.

Nuisance regression. Additional preprocessing consists of regressing out the grey matter, ventricle and white matter average signal, and the movement between frames from the six image alignment parameters x, y, z, θ_x , θ_y, and θ_z on the actual and the previous TR and their squares, which correspond to the Volterra series expansion of motion (Power et al. 2014; Friston et al. 1996; Power et al. 2012). The regression's coefficients (beta weights) are calculated solely based on frames with low movement, but regression is calculated considering all the frames to preserve temporal order in the data for filtering in the time domain. Next, timecourses are filtered using a first order Butterworth band pass filter to preserve frequencies between 0.009 and 0.080 *Hz*.

HCP: For this analysis, we used the ICA-FIX denoised rfMRI timecourses provided by the HCP. These timecourses were minimally processed first by the HCP as described below. Next, they applied Independent Component Analysis (ICA) to account for nuisance and covariates with a new FSL tool named FIX that automatically removes artifactual or "bad" components. Briefly, each voxel's timecourses from 25 HCP subjects were decomposed into 229 spatial components. Of these, on average 24 components were hand-classified as "good" and the remainder as "bad". Next, a classifier was trained to identify "good" and "bad" components. Once the classifier was optimized (by leave-one-subject-out cross validation), the resulting classifier was used to identify

the “bad” components from each participant. Such components were removed by regressing the “bad” components (timecourses) out from the timecourses on each grayordinate.

Machine learning based identification of siblings

Classifiers: For each run (out of *N*), SVM classifiers with a Gaussian (or Radial Basis Function, RBF) were optimized by leave-one-out cross validation (loocv), unless otherwise stated. The optimization is calculated using gradient descent to minimize the out of sample classification error by optimizing the parameters "Box Constraint" and a "scaling factor" ("Kernel Scale") in SVM. For SVM, “Box Constraint” controls the maximum penalty imposed on margin-violating observations, and helps in preventing overfitting (regularization) (Abu-Mostafa et al. 2012). This parameter is directly related to the number of support vectors used for classification. Increasing this number decreases the number of support vectors at the cost of training time. “Kernel Scale**”** is a scaling factor applied to the predictor variables.

Estimation of single-subject functional organization using traditional functional connectivity correlation matrix

Correlation matrices were calculated for each participant included in this study by calculating the Pearson correlation coefficient of the BOLD activity (after motion censoring) for any pair of ROIs used on each parcellation schema. The result was a ROI×ROI correlation matrix *per* participant that were used to characterize individual FC. To compare each scan pair, we defined the “spatial correlation” per ROI as the correlation between two subjects’ FC vectors, where each vector is simply the set of correlations between that ROI and every other ROI.

Features for SVM using traditional correlations: To extract a comparable feature set using the pearson correlation matrices, we defined the “spatial correlation” per ROI as the correlation

between two subjects' FC vectors, where each vector is simply the set of correlations between that ROI and every other ROI.

Heritability Analysis:

Traditional heritability: Because our heritability approach differs from prior studies, it was important to estimate the heritability of individual functional connections using traditional approaches from the literature as well. Therefore, the heritability of traditional correlations was tested using generalized linear mixed models (Visscher and Goddard, 2015) via the "fitlmematrix" function in MATLAB, where each functional correlation was used as the predicted measure. For comparisons to the SVM model (see: Figure 2), mean ROI heritability was calculated for each ROI by taking the average heritability for functional correlations between the given ROI and all other ROIs. Mean network heritability was measured by computing the average of the mean ROI heritability for all ROIs within each network. All measures were transformed into normally distributed variables using a rank-based transform (Glahn et al., 2010). To aid in computation and reduce the dimensionality of the data, eigenvectors, derived via singular value decomposition, from the kinship and shared environment matrices were random factors. Per matrix, an eigenvector exists per subject and represents the shared genetics or environment between that subject and every other subject. The kinship matrix represents the genetic correlation between each pair of subjects; monozygotic twins have a genetic correlation of 1, other siblings have a correlation of 0.5, while unrelated pairs have no correlation; the kinship matrix is doubled prior to being used as a random factor. The shared environment matrix was generated as a binary matrix where a 1 indicated that the given pair of subjects lived in the same household and a 0 indicated that the given pair lived in

separate households. Sex and age were used as fixed effects in the analysis. Model parameters were estimated using restricted maximum likelihood estimation. To determine whether the genetic associations significantly explained variance in functional connections, another mixed model, called the shared environment model, was tested that excluded the kinship factor. A chi-squared test of the difference in log likelihood between the two types of models determined whether the contribution of the genetic component was statistically significant. We used the false discovery rate (FDR) to correct for multiple comparisons (Benjamini and Hochberg, 1995). Point estimates of heritability were calculated from the genetic plus shared environment model by measuring the ratio of the genetic component variance to the total variance (Visscher and Goddard, 2015).

Supplemental figures.

Figure 1- Figure Supplement 1. Visualizing functional networks using connectotyping and traditional correlations. Panel a) shows the mean connectotype across individuals; panel b) shows a connectoype from 1 individual; and panel c) shows the correlation matrix of that individual. The "*y"* axis correspond to each ROI, sorted per functional network. The number shown in the "*y*" axis corresponds to the network's index, as coded in the table at the side.

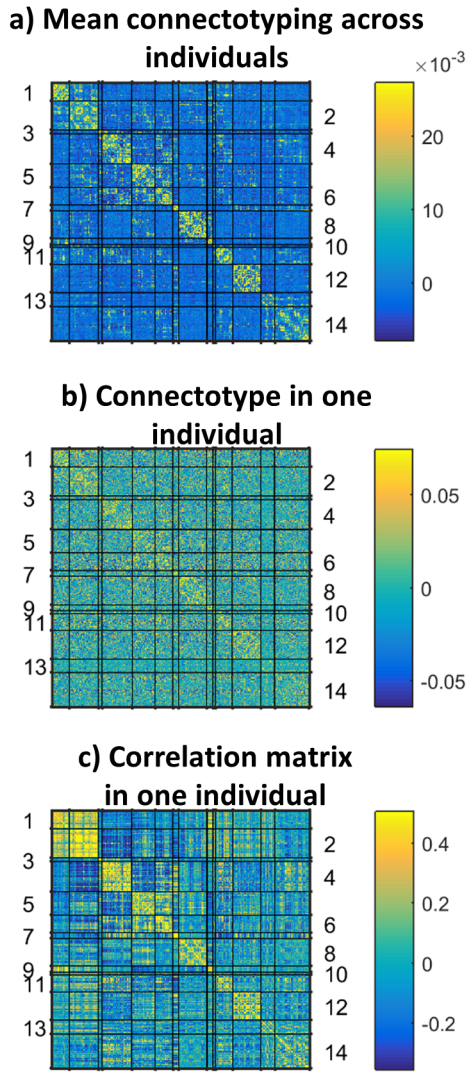

1) Auditory
2) Cingulo Opercular
3) Cingulo Parietal
4) Default
5) Dorsal Attention
6) Fronto-Parietal
7) Retrosplenial Temporal
8) Somato-sensory mouth
9) Somato-sensory hand
10) Salience
11)Ventral-Attention
12) Visual
13) Subcortical
14) No-assignment

Figure 1- Figure Supplement 2. Average correlation prediction when predicting timecourses from the same participant but months later. This figure corresponds to the group II from the figure I. This group is highlighted here to show in greater detail the low association between the average correlation coefficient of predicted timecourses and time between scans for connectotyping. This figure highlights the correlation coefficient between the average similarities between scans and time between scans following 3 criteria: 1) using all the data; 2) time between scans <=1.5 years; and 3) time between scans >1.5 years.

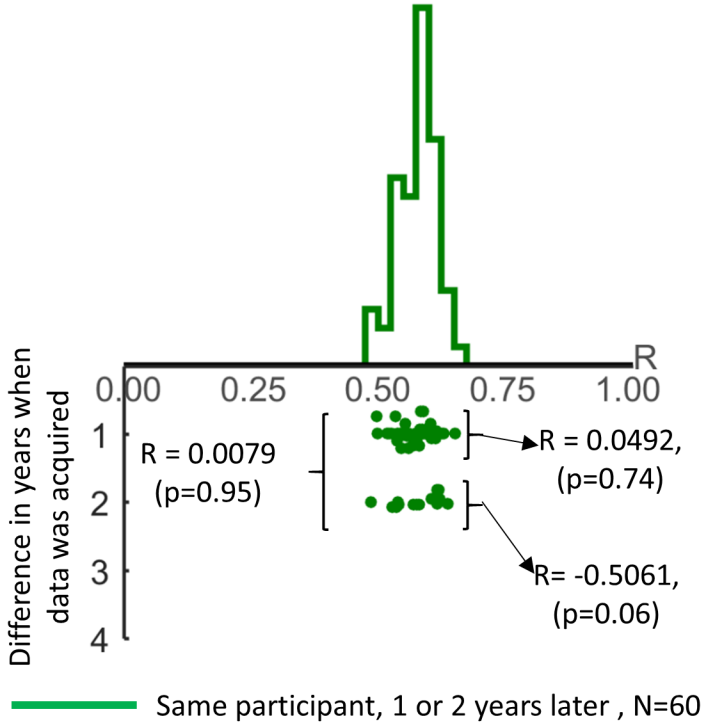

Figure 1-Figure Supplement 3. Segregating groups of paired data (same scan, same participant, siblings and unrelated) by predicting timecourses and spatial correlations. Panels "a" to "e" show the average correlation coefficient between predicted and observed timecourses across all participants under different parcellation schemas. Groups are based on the dataset used to calculate the model used in the prediction: I) the same scan session, II) the same participant but in a different scan session, III) a sibling, and IV) from unrelated individuals. Each panel also show the differences in age (measured in years) between each paired-data.

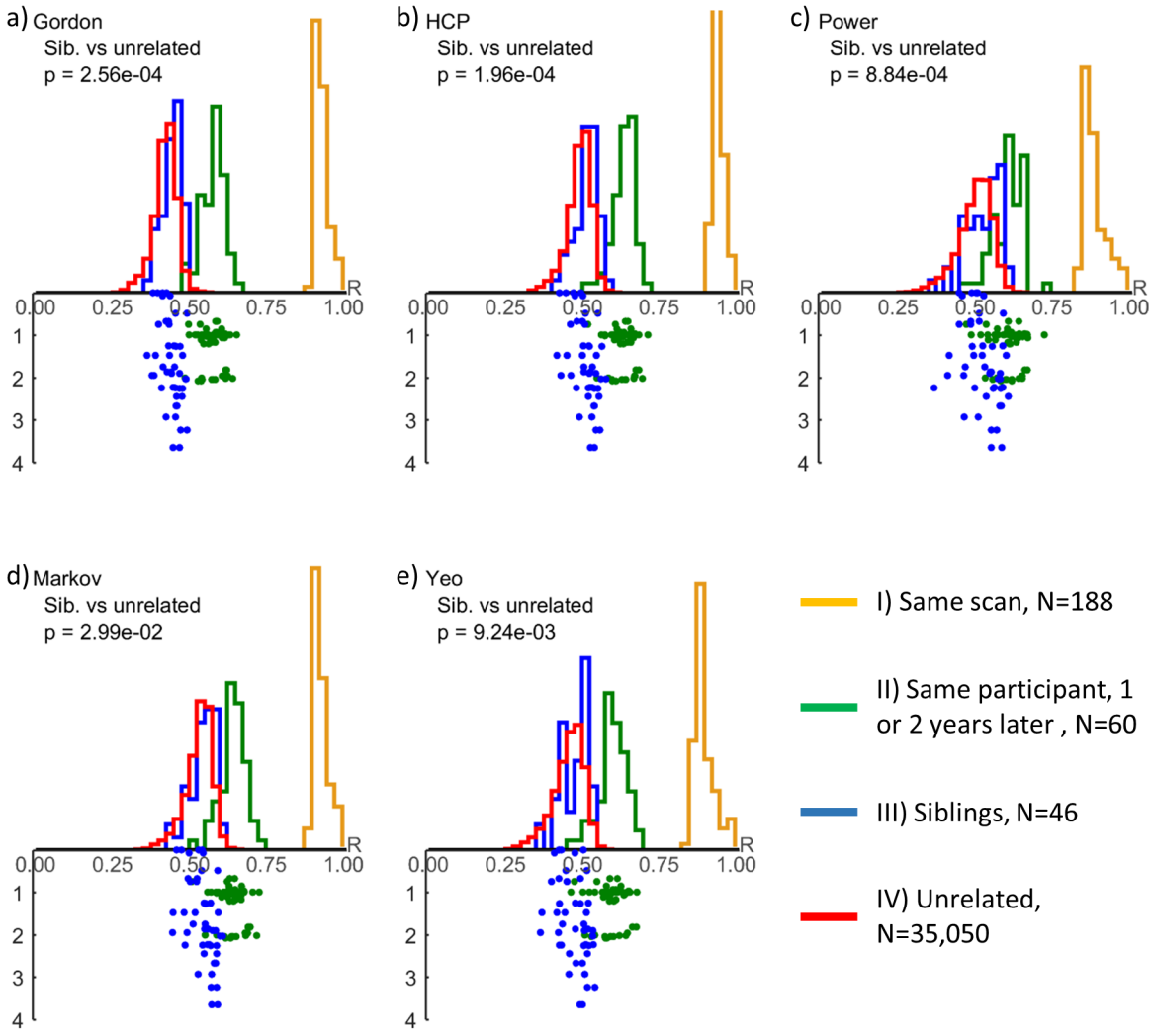

Figure 1-Figure Supplement 4. Spatial correlations. Panel a shows the results for connectotyping predicting timecourses and is repeated here for reference. Panels b and c show the spatial correlations using the Gordon parcellation for connectotyping (b) and traditional correlation matrices (c).

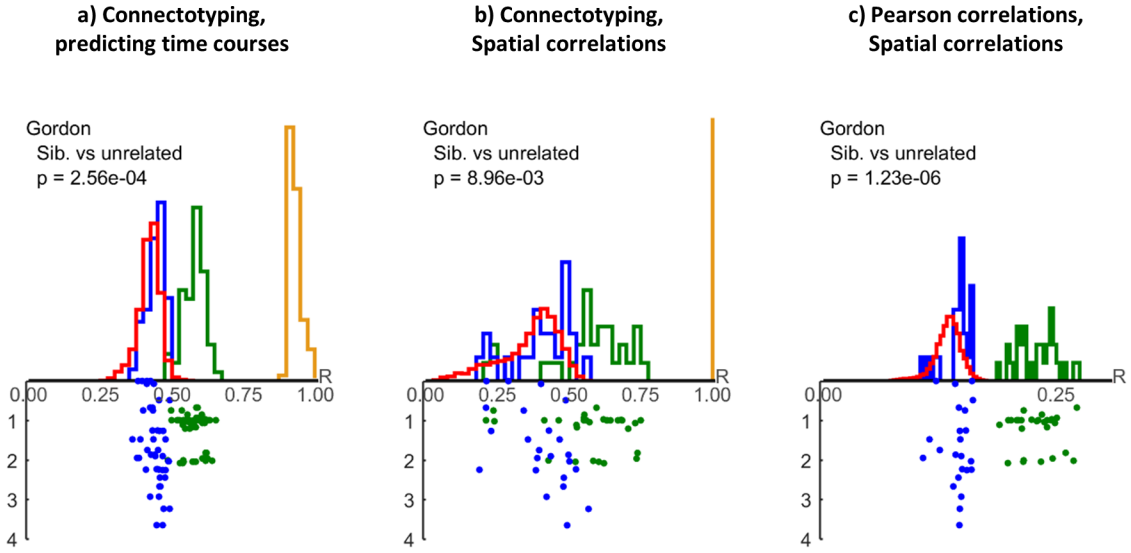

Figure 3-Figure Supplement 1. Top ROIs per functional network. Panel a) shows their location in a cartoon's brain. Panel b) shows the top features sorted per functional network (as in Figure 3). Panel c) shows the same top 100 ROIs sorted as the ratio of the number of ROIs identified in the network relative to the given network's size.

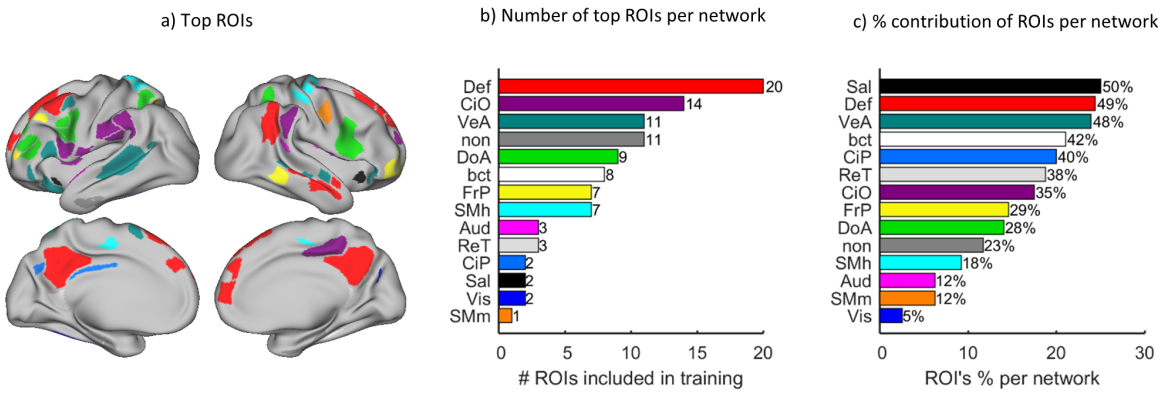

Figure 3-Figure Supplement 2. Mapping the 11 ROIs (within the top 100) with no proper assignment in Gordon into Yeo. Panel a shows the 11 ROIs within the top 100 with no functional assignment on top of the functional communities as defined by Yeo (Yeo et al., 2011) (also see tables S2 and S3). Colorcode shown in the bottom. Panel b shows the same information into a spherical projection of the brain.

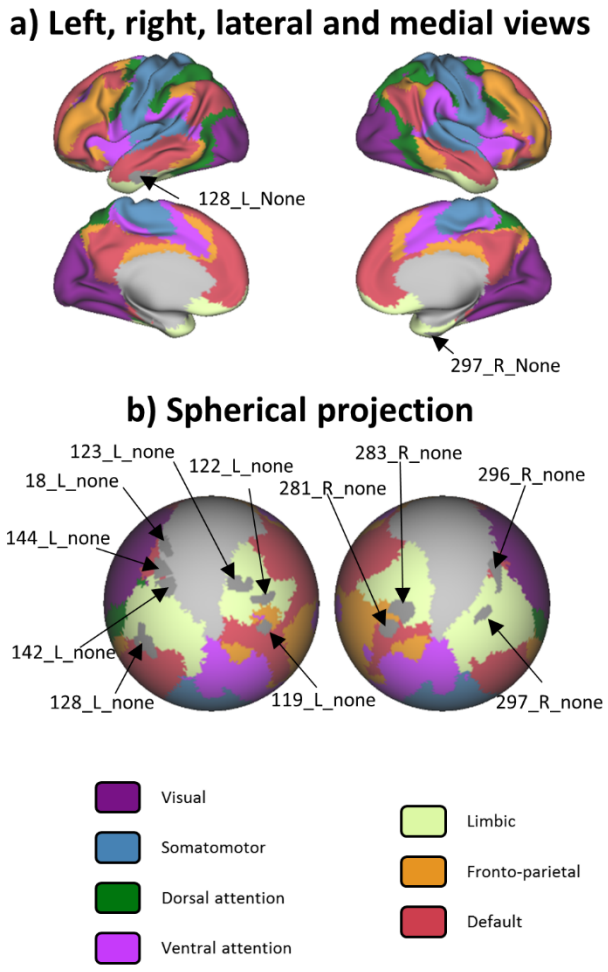

Figure 3-Figure Supplement 3. Distributions of ROI's size for the Gordon (+ subcortical) parcellation schema. Panel a) shows the distribution of the top 100 ROIs size (black) and the remaining 252 (red), as accounted by their number of grayordinates (see Table S2). Panel b) splits such distributions *per* functional network.

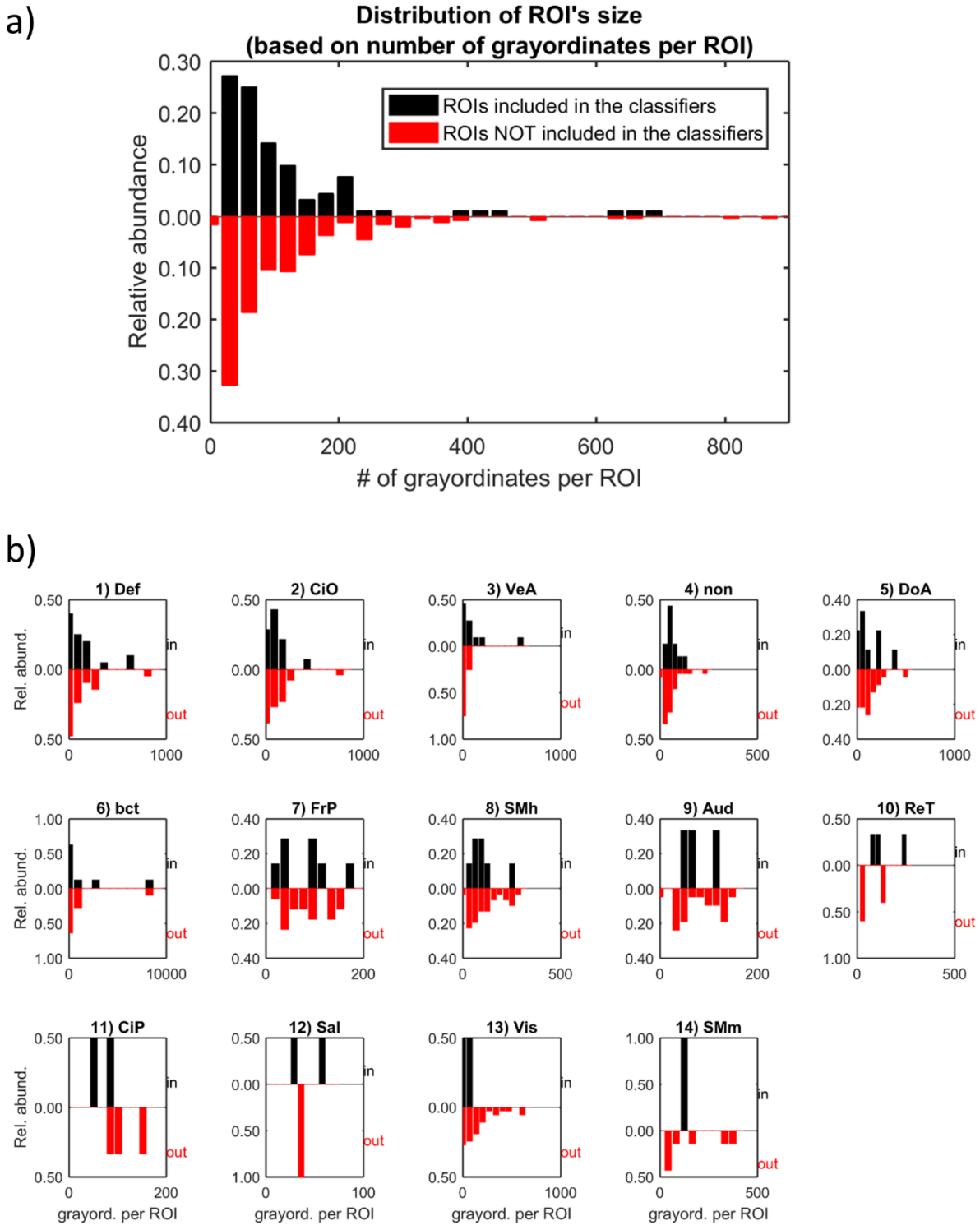

Figure 3-Figure Supplement 4. SVM's out of sample performance for CONNECTOTYPING and correlations, N=1000 per feature set. Mean full accuracy (+), mean accuracy predicting siblings (•), and mean accuracy predicting unrelated population (□). Panel A shows the out of sample performance of the SVM classifiers for connectotyping as a function of the number of features (x-axis) used for classification. Left-most panel shows the average results as a function of the number of features used for classification. Right-side subpanels show the distributions of accuracy, specificity (accuracy predicting siblings), and specificity (accuracy predicting unrelated participants) compared with the null hypothesis. Panel B show the corresponding results for connectotyping when the features were selected by functional network, as defined by Gordon (See Figure 2).

A. Connectotyping, per top features, out of sample accuracy.

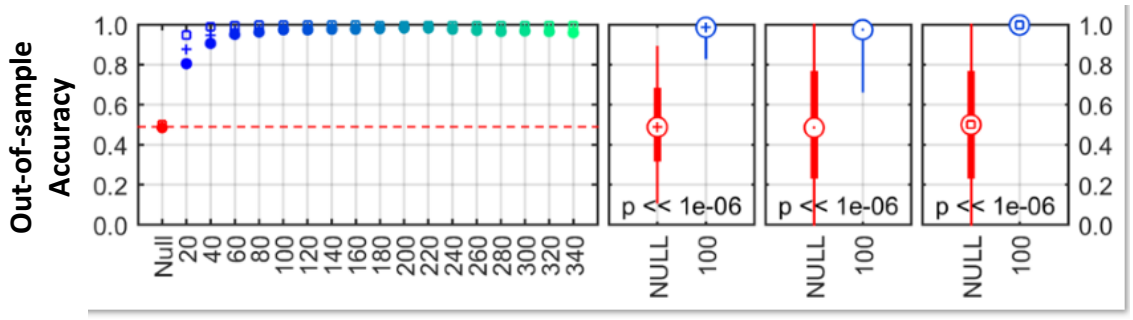

B Connectotyping, per network, out of sample accuracy.

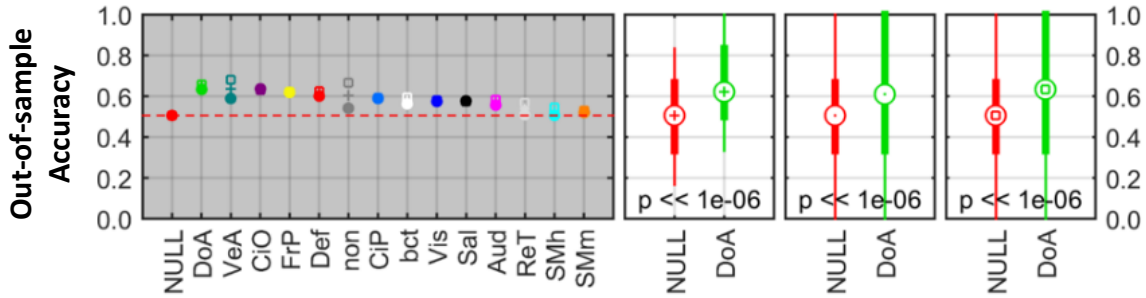

Figure 3 –Figure Supplement 5. Classifying siblings vs unrelated populations when other sibling pairs of the same family are included in the training set (sample of youths) characterizing brain connectivity using Pearson correlations. Distributions of (A) full accuracy, (B) siblings, and (C) unrelated pairs for the SVM when traditional correlations are used to characterize brain connectivity. The bottom left panel shows the consensus' ROI's per functional network (as defined by Gordon) used in the classifier, and the location of such ROIs in the surface of the brain. Each distribution highlights the percentiles 2.5 and 97.5 with a thin line. Thick lines are used to highlight the percentiles 25 and 75 while the central markers are used to show the mean values. Red distributions correspond to the null distributions.

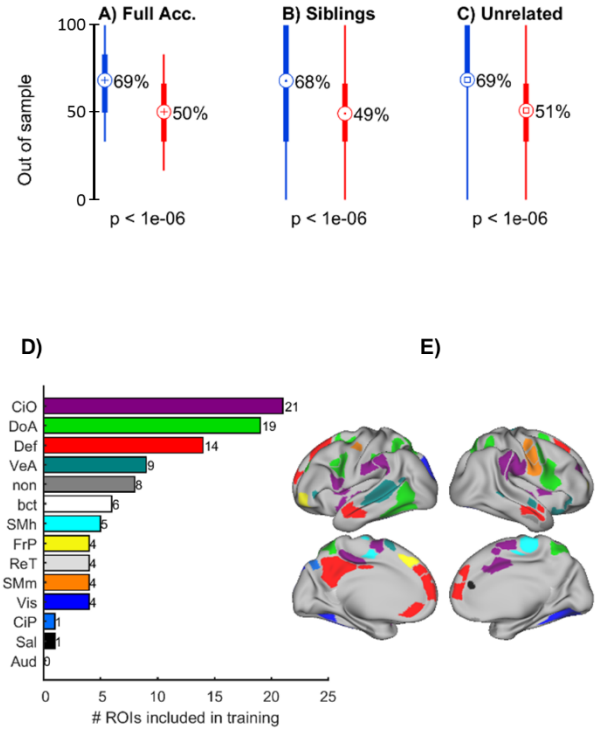

Figure 3-Figure Supplement 6. SVM's out of sample performance for CORRELATIONS, N=1000 per feature set. Mean full accuracy (+), mean accuracy predicting siblings (•), and mean accuracy predicting unrelated population (□). Panel A shows the out of sample performance of the SVM classifiers for correlations as a function of the number of features (x-axis) used for classification. Left-most panel shows the average results as a function of the number of features used for classification. Right-side subpanels show the distributions of accuracy, specificity (accuracy predicting siblings), and specificity (accuracy predicting unrelated participants) compared with the null hypothesis. Panel B show the corresponding results for correlations when the features were selected by functional network, as defined by Gordon (See Figure 2).

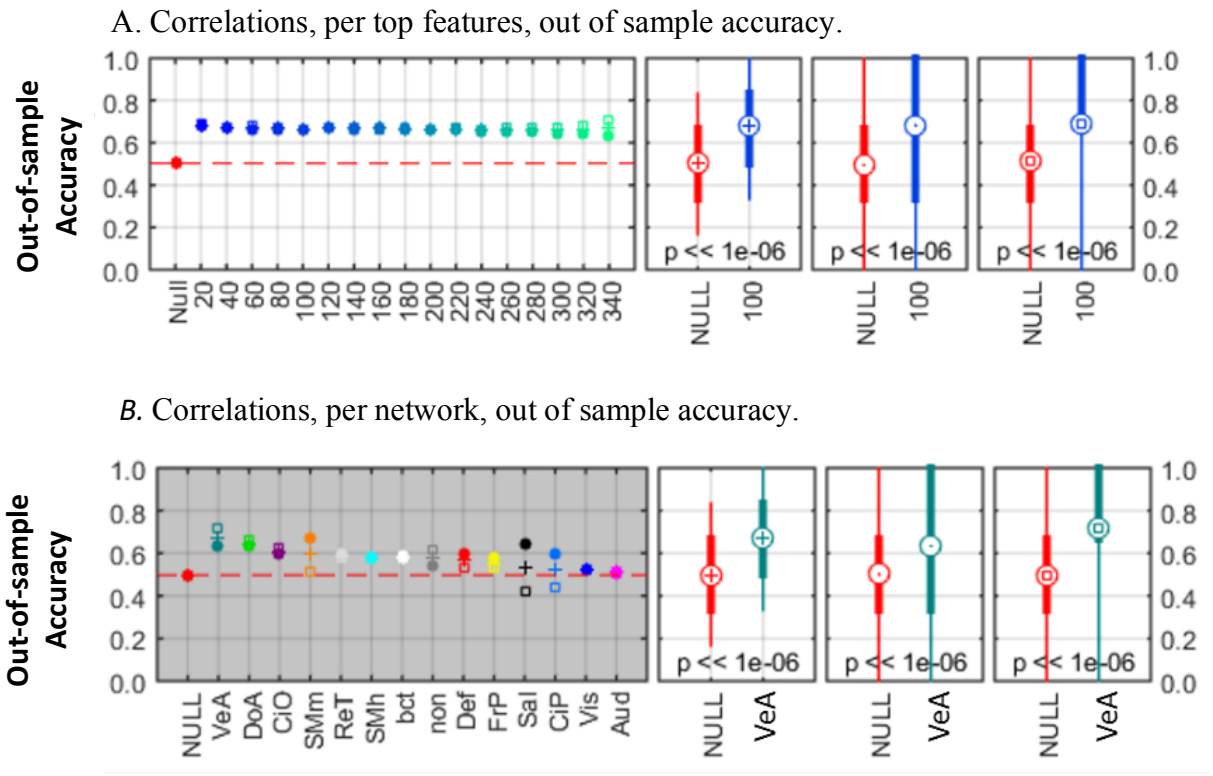

Figure 4-Figure Supplement 1. Classifying siblings vs unrelated populations (N=100 per feature set) using connectotyping and the entire HCP dataset (N=499). Panel A show the mean full accuracy (+), mean accuracy predicting siblings (•), and mean accuracy predicting unrelated population (□) using the correlation coefficient of model-based connectivity matrices (connectotyping) as features. The number of features used for classification were 20, 40, … 340. Analysis was repeated 100 times per feature set. (B-G) shows the distributions of (B) full accuracy, (C) siblings, (D) unrelated, (E) monozygotic, (F) dizygotic, and (G) non-twin sibling pairs for the connectotyping-based SVM classifier.

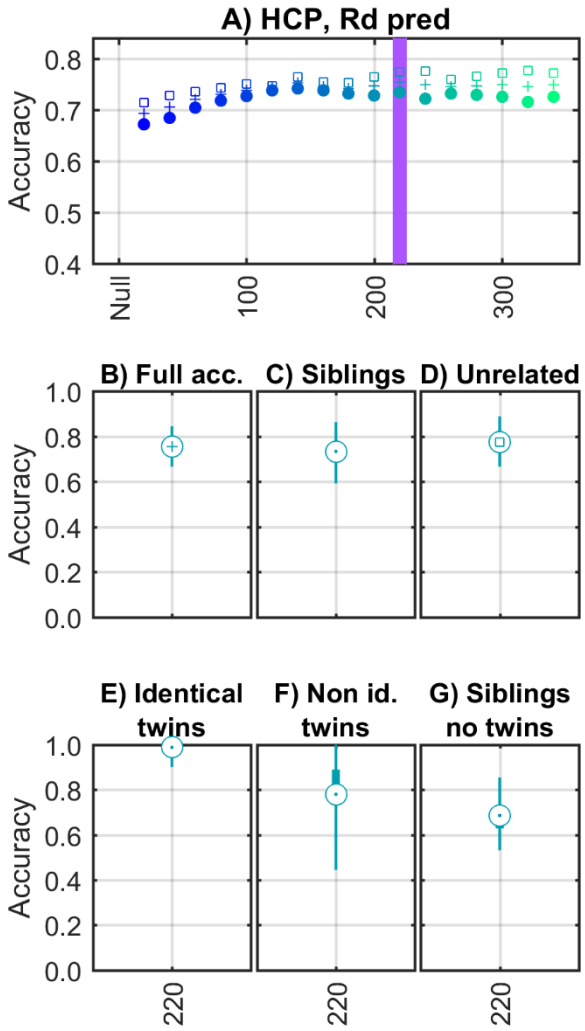

Figure 4-Figure Supplement 2. Classifying siblings vs unrelated populations (N=1000 per feature set), when families with twins and other sibling pairs of the same family were NOT included in the training set (HCP dataset) using a high quality subsample of N=198 scans, using CONNECTOTYPING predicting timecourses. Panel A show the mean full accuracy (+), mean accuracy predicting siblings (•), and mean accuracy predicting unrelated population (□) using the correlation coefficient of model-based connectivity matrices (connectotyping) as features. The number of features used for classification were 20, 40, … 340. Analysis was repeated 1,000 times. (B-G) shows the distributions of (B) full accuracy, (C) siblings, (D) unrelated, (E) monozygotic, (F) dizygotic, and (G) non-twin sibling pairs for the connectotyping-based SVM classifier.

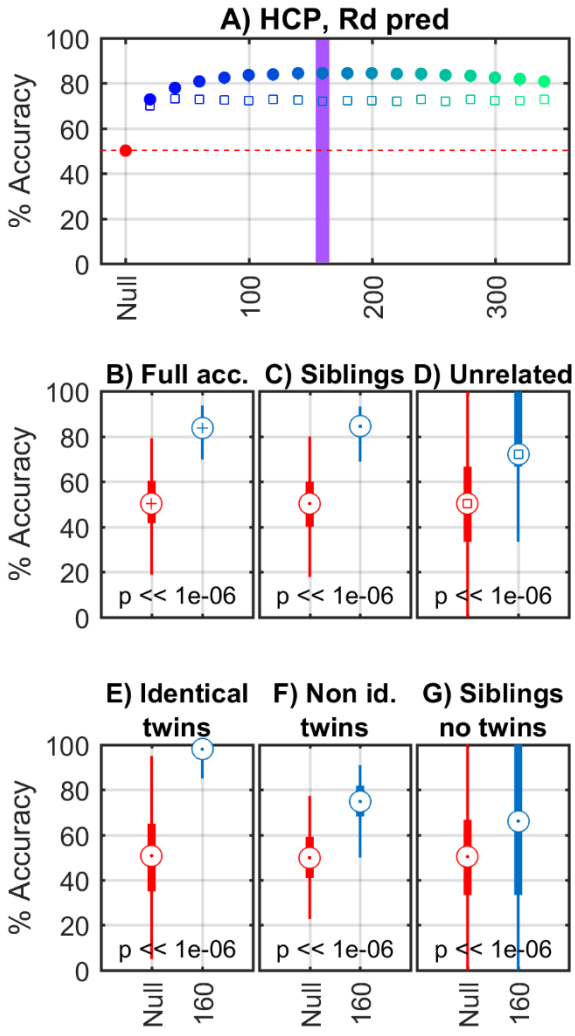

Figure 4-Figure Supplement 3. Classifying siblings vs unrelated populations, when families with twins and other sibling pairs of the same family were NOT included in the training set (HCP dataset) using correlations. Distributions of (A) full accuracy, (B) siblings, (C) unrelated, (D) monozygotic, (E) dizygotic, and (F) non-twin sibling pairs for the correlations-based SVM classifier. (G) The consensus' distribution of ROI's per functional network used in the classifier. (H) The location of such ROIs in the surface of the brain. Each distribution highlights the percentiles 2.5 and 97.5 with a thin line. Thick lines are used to highlight the percentiles 25 and 75 while the central markers are used to show the mean values. Red distributions correspond to the null distributions.

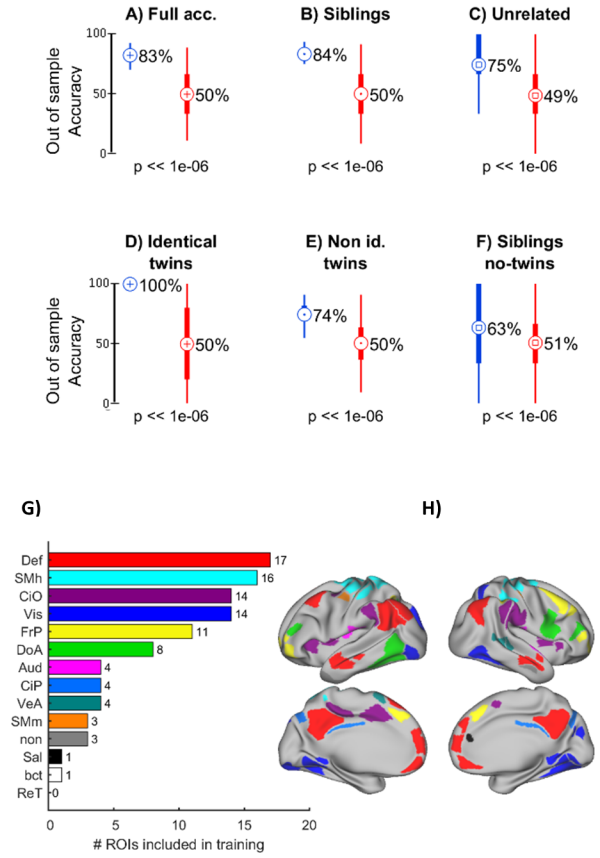

Figure 4-Figure Supplement 4. Classifying siblings vs unrelated populations (N=1000 per feature set), when families with twins and other sibling pairs of the same family were NOT included in the training set (HCP dataset) using a high quality subsample of N=198 scans, using traditional CORRELATIONS to characterize brain connectivity. Panel A show the mean full accuracy (+), mean accuracy predicting siblings (•), and mean accuracy predicting unrelated population (□) using the correlation coefficient of model-based connectivity matrices (connectotyping) as features. The number of features used for classification were 20, 40, … 340. Analysis was repeated 1,000 times. (B-G) shows the distributions of (B) full accuracy, (C) siblings, (D) unrelated, (E) monozygotic, (F) dizygotic, and (G) non-twin sibling pairs for the connectotyping-based SVM classifier.

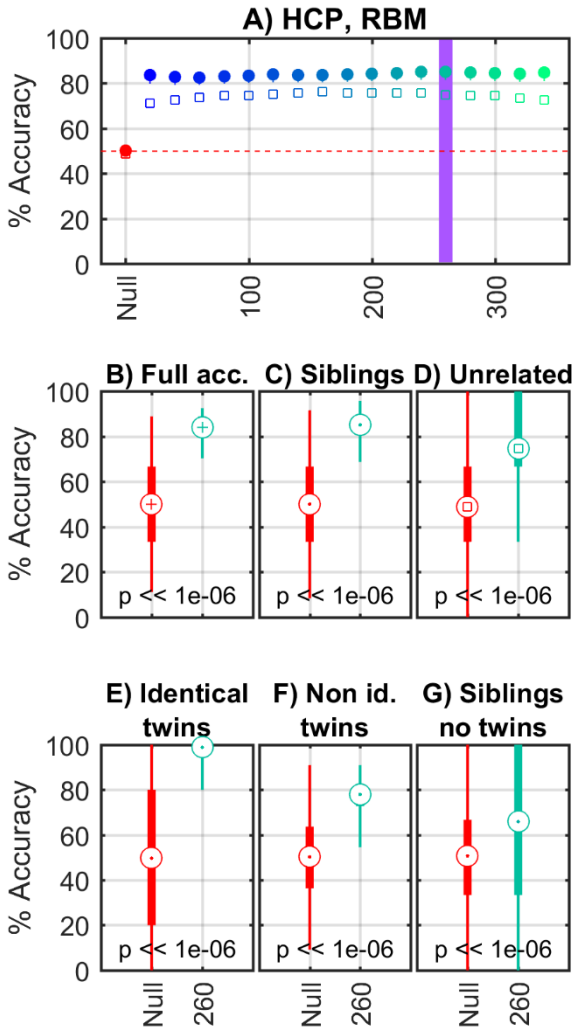

Figure 5-Figure Supplement 1. Dataset 1 predicting dataset 2 using connectotyping. Distributions of out-of-sample accuracies (N=1000 per feature set) when classifiers were trained in one dataset (OHSU, ie youth, or HCP, ie adults) and tested in the other dataset.

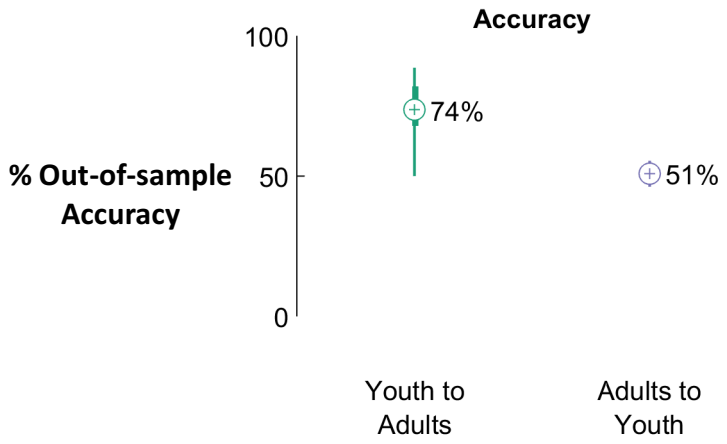

Figure 5-Figure Supplement 2. Dataset 1 predicting dataset 2 using traditional correlations. Distributions of out-of-sample accuracies (N=1000 per feature set) when classifiers were trained in one dataset (OHSU, ie youth, or HCP, ie adults) and tested in the other dataset.

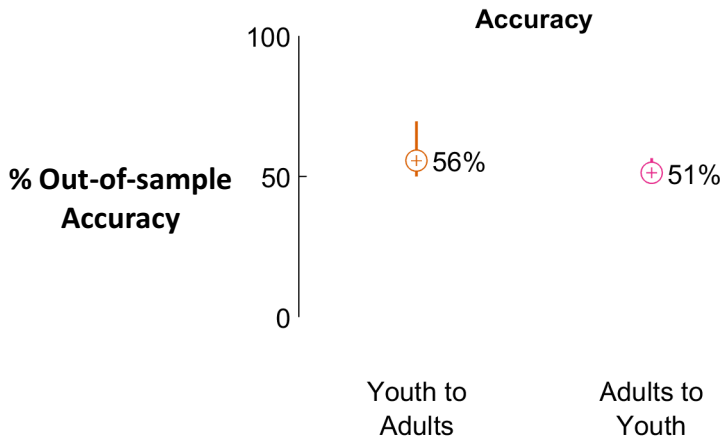

Figure 6-Figure Supplement 1. Out of sample performance of classifiers using connectotyping (green) and different anatomical features (brown) to classify kinship in adults when classifiers were trained using data from an independent dataset of youths. Green traces correspond to the results of the classification using connectotyping, as shown in figures 5 and 6. Same classification procedure was repeated using cortical thickness and sulcal depth as features (after removing the effect of head size by normalization of regression), but using the top 100 more distinct features according to connectotyping (light brown, labeled as "Comb" to indicate "Combined"). Dark brown lines show the performance of the classifiers when features and feature selection was based on anatomical features.

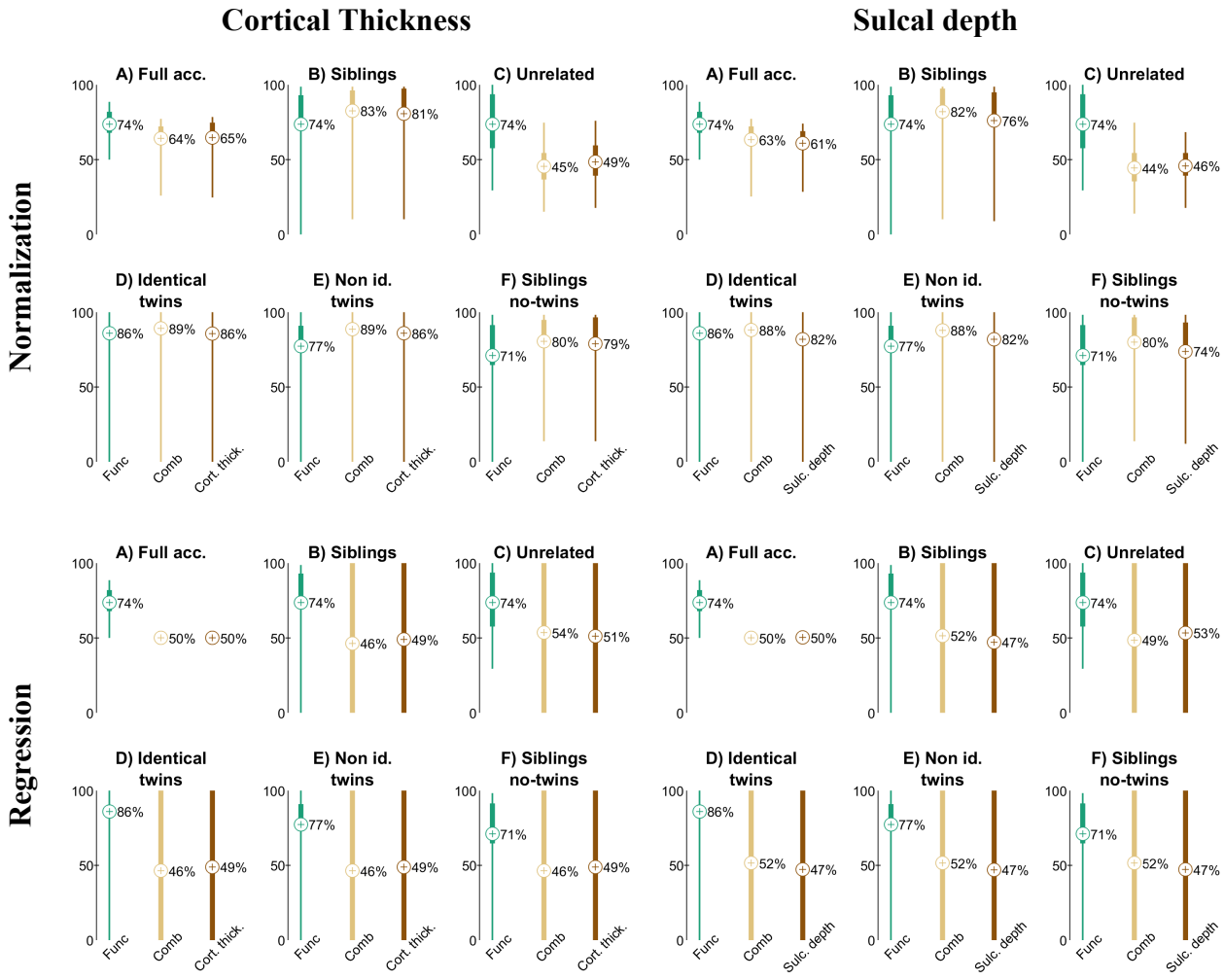

Figure 7-Figure Supplement 1. Summary of heritability (circle) and shared environment (plus sign) analyses conducted on 198 (red) and 499 (blue) participants (connectotyping).

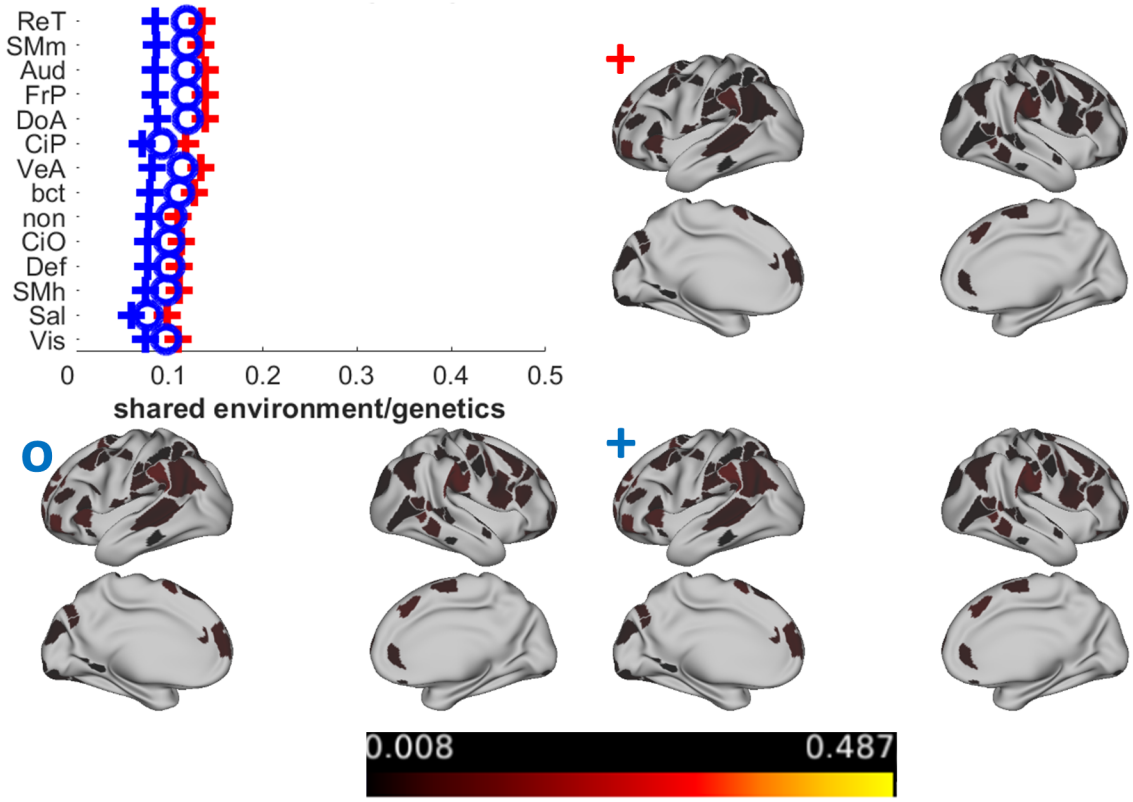

+ - shared environment 198 participants
+ - shared environment 499 pariticipants
o – shared genetics 499 participants

Figure 7-Figure Supplement 2. Heritability traditional functional connectivity correlations

(7A) The Spatial correlation's heritability of the top 100 regions used in the SVM classification for Traditional correlations (see: Figure 3-Figure Supplement 5). (Panel B) The spatial correlation heritability for each network. Networks are sorted from most to least heritable, and the bar color matches the networks shown in figure 2.

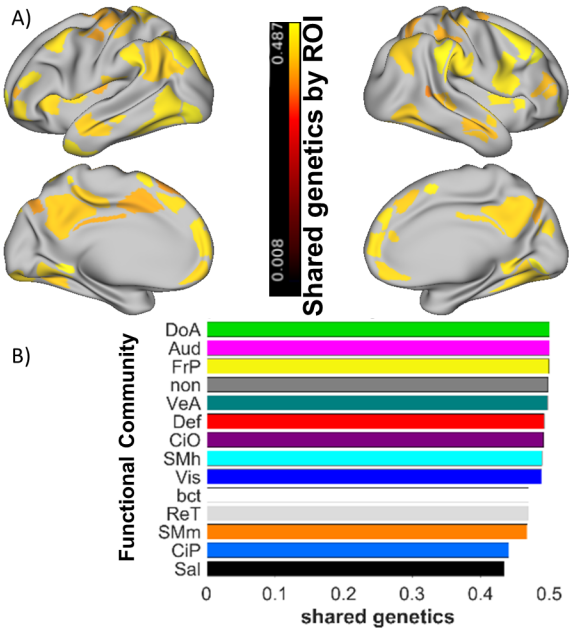

Figure 7-Figure Supplement 3. Summary of heritability (circle) and shared environment (plus sign) analyses conducted on 198 (red) and 499 (blue) participants for spatial correlations. Traditional heritability (black circle) and shared environment (black plus sign) on traditional correlations are also shown.

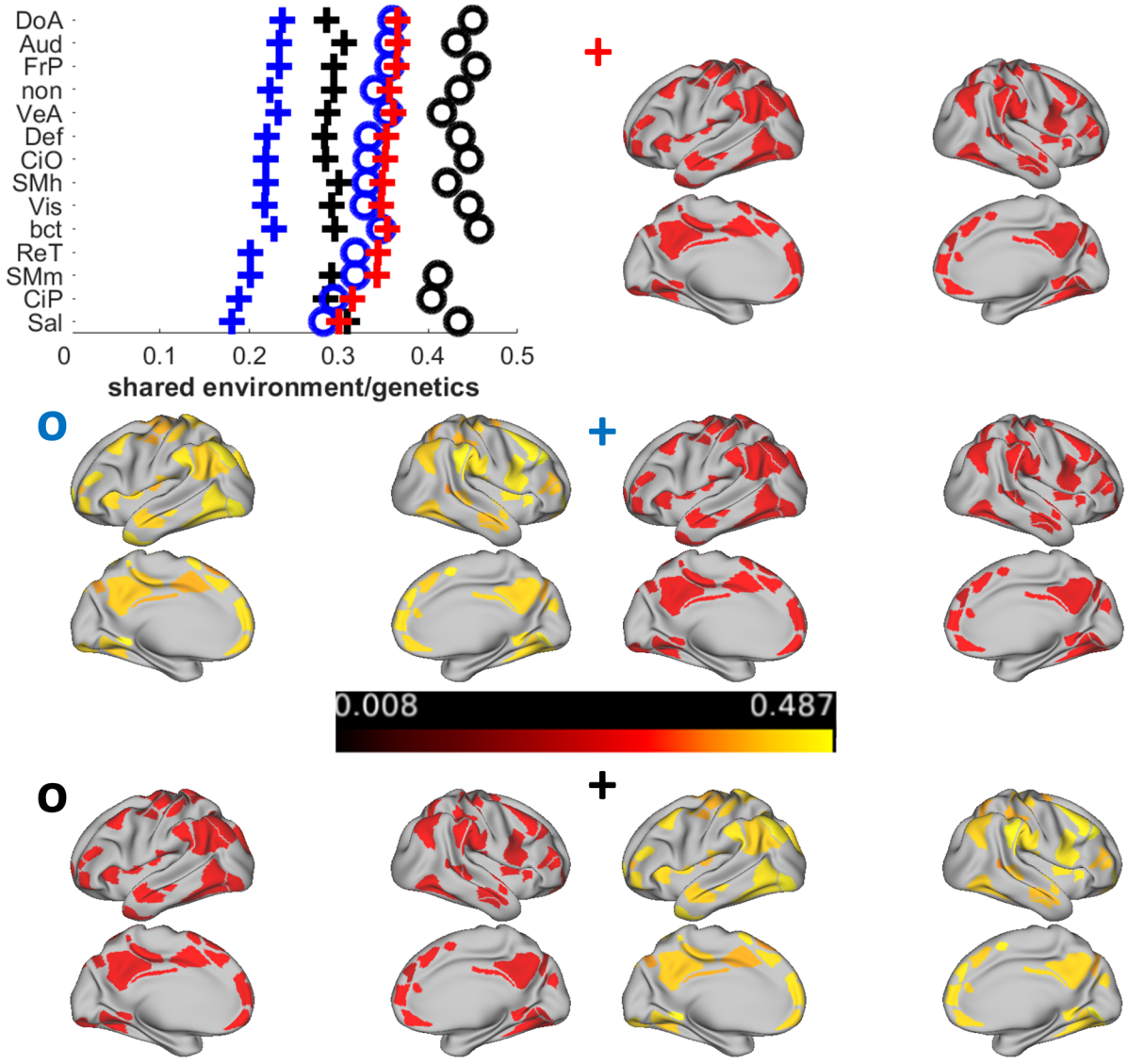

+ - shared environment 198 participants
+ - shared environment 499 pariticipants
+ - GLMM shared environment 198 participants for top 100 ROIs
o – shared genetics 499 participants
o – GLMM shared genetics 198 participants for top 100 ROIs

Supplemental tables.

Table S1. Siblings included in the study

Family	Siblings *per* family	Scans *per* sibling		Correlations of connectivity matrices *per* family	Predictions *per* family
1	2	2	1	2	4
2	2	1	1	1	2
3	2	1	1	1	2
4	2	2	2	4	8
5	2	1	3	3	6
6	2	1	1	1	2
7	2	1	2	2	4
8	2	1	1	1	2
9	2	1	1	1	2
10	2	1	1	1	2
11	2	1	1	1	2
12	2	1	1	1	2
13	2	1	1	1	2
14	2	1	1	1	2
15	2	1	1	1	2
16	2	1	1	1	2
		Total		**23**	**46**

Table S2. Ranking of the individuals ROIs to differentiate between siblings and unrelated.

Index	ROI name	Network	Number of grayordinates
1	155_L_DorsalAttn	L DoA	72
2	200_R_Default	R Def	194
3	240_R_FrontoParietal	R FrP	104
4	144_L_None	L non	74
5	219_R_CinguloOperc	R CiO	218
6	PALLIDUM_RIGHT	Subct	260
7	75_L_VentralAttn	L VeA	104
8	74_L_DorsalAttn	L DoA	86
9	153_L_CinguloOperc	L CiO	84
10	60_L_VentralAttn	L VeA	49
11	103_L_CinguloOperc	L CiO	95
12	295_R_RetrosplenialTemporal	R ReT	87
13	110_L_DorsalAttn	L DoA	85
14	113_L_DorsalAttn	L DoA	42
15	4_L_Default	L Def	163
16	25_L_Default	L Def	84
17	146_L_Default	L Def	99
18	165_R_Default	R Def	161
19	89_L_CinguloParietal	L CiP	54
20	281_R_None	R non	76
21	122_L_None	L non	57
22	44_L_Default	L Def	223
23	119_L_None	L non	42
24	157_L_Default	L Def	147
25	106_L_DorsalAttn	L DoA	239
26	222_R_VentralAttn	R VeA	58
27	277_R_FrontoParietal	R FrP	104
28	290_R_Default	R Def	223
29	18_L_None	L non	62
30	79_L_VentralAttn	L VeA	50
31	158_L_VentralAttn	L VeA	70
32	170_R_FrontoParietal	R FrP	116
33	331_R_Default	R Def	30
34	262_R_DorsalAttn	R DoA	130
35	51_L_DorsalAttn	L DoA	231
36	HIPPOCAMPUS_LEFT	Subct	764
37	194_R_SMhand	R SMh	34
38	BRAIN_STEM	Subct	3472

Index	ROI name	Network	Number of grayordinates
39	230_R_Auditory	R Aud	57
40	37_L_SMhand	L SMh	70
41	174_R_RetrosplenialTemporal	R ReT	257
42	23_L_VentralAttn	L VeA	84
43	296_R_None	R non	77
44	14_L_RetrosplenialTemporal	L ReT	128
45	333_R_VentralAttn	R VeA	43
46	332_R_VentralAttn	R VeA	44
47	154_L_Default	L Def	59
48	12_L_CinguloParietal	L CiP	93
49	63_L_CinguloOperc	L CiO	226
50	220_R_Default	R Def	444
51	225_R_Default	R Def	85
52	AMYGDALA_LEFT	Subct	315
53	PUTAMEN_RIGHT	Subct	1010
54	322_R_Default	R Def	188
55	101_L_CinguloOperc	L CiO	85
56	2_L_SMhand	L SMh	275
57	164_R_SMmouth	R SMm	132
58	198_R_CinguloOperc	R CiO	81
59	50_L_SMhand	L SMh	119
60	108_L_FrontoParietal	L FrP	43
61	316_R_Default	R Def	55
62	242_R_VentralAttn	R VeA	132
63	83_L_Salience	L Sal	32
64	80_L_VentralAttn	L VeA	236
65	180_R_CinguloOperc	R CiO	459
66	112_L_CinguloOperc	L CiO	159
67	283_R_None	R non	106
68	325_R_Default	R Def	75
69	CEREBELLUM_LEFT	Subct	8709
70	239_R_Auditory	R Aud	82
71	238_R_CinguloOperc	R CiO	134
72	156_L_Default	L Def	54
73	247_R_Salience	R Sal	62
74	107_L_DorsalAttn	L DoA	49
75	HIPPOCAMPUS_RIGHT	Subct	795
76	7_L_FrontoParietal	L FrP	35
77	317_R_CinguloOperc	R CiO	48

Index	ROI name	Network	Number of grayordinates
78	320_R_FrontoParietal	R FrP	44
79	160_L_Auditory	L Aud	122
80	123_L_None	L non	82
81	62_L_VentralAttn	L VeA	645
82	136_L_Visual	L Vis	80
83	315_R_Default	R Def	115
84	297_R_None	R non	44
85	274_R_CinguloOperc	R CiO	114
86	217_R_SMhand	R SMh	91
87	162_R_Default	R Def	674
88	105_L_CinguloOperc	L CiO	208
89	311_R_Visual	R Vis	35
90	147_L_CinguloOperc	L CiO	30
91	275_R_DorsalAttn	R DoA	405
92	96_L_FrontoParietal	L FrP	181
93	PALLIDUM_LEFT	Subct	297
94	205_R_SMhand	R SMh	103
95	142_L_None	L non	71
96	201_R_SMhand	R SMh	140
97	81_L_CinguloOperc	L CiO	45
98	128_L_None	L non	137
99	324_R_Default	R Def	66
100	1_L_Default	L Def	715
101	182_R_FrontoParietal	R FrP	97
102	236_R_DorsalAttn	R DoA	104
103	54_L_SMhand	L SMh	70
104	286_R_None	R non	35
105	139_L_Visual	L Vis	148
106	30_L_SMhand	L SMh	35
107	39_L_SMmouth	L SMm	63
108	93_L_CinguloParietal	L CiP	118
109	184_R_Default	R Def	132
110	280_R_None	R non	66
111	138_L_Visual	L Vis	57
112	292_R_None	R non	246
113	127_L_Default	L Def	295
114	73_L_None	L non	129
115	78_L_FrontoParietal	L FrP	145
116	109_L_FrontoParietal	L FrP	151

Index	ROI name	Network	Number of grayordinates
117	234_R_CinguloOperc	R CiO	184
118	221_R_VentralAttn	R VeA	61
119	DIENCEPHALON_VENTRAL_RIGHT	Subct	712
120	159_L_None	L non	70
121	266_R_DorsalAttn	R DoA	42
122	173_R_CinguloParietal	R CiP	90
123	199_R_DorsalAttn	R DoA	67
124	150_L_Default	L Def	280
125	71_L_CinguloOperc	L CiO	152
126	43_L_DorsalAttn	L DoA	56
127	254_R_CinguloParietal	R CiP	159
128	111_L_CinguloOperc	L CiO	102
129	91_L_DorsalAttn	L DoA	198
130	270_R_SMhand	R SMh	117
131	212_R_SMmouth	R SMm	361
132	21_L_CinguloOperc	L CiO	326
133	318_R_CinguloOperc	R CiO	164
134	287_R_None	R non	89
135	114_L_Default	L Def	41
136	181_R_CinguloOperc	R CiO	44
137	90_L_Visual	L Vis	83
138	214_R_SMhand	R SMh	128
139	243_R_VentralAttn	R VeA	123
140	92_L_DorsalAttn	L DoA	52
141	THALAMUS_LEFT	Subct	1288
142	267_R_Visual	R Vis	92
143	61_L_VentralAttn	L VeA	42
144	206_R_SMhand	R SMh	43
145	314_R_None	R non	37
146	64_L_Auditory	L Aud	46
147	223_R_CinguloOperc	R CiO	829
148	ACCUMBENS_LEFT	Subct	135
149	258_R_Visual	R Vis	81
150	185_R_CinguloOperc	R CiO	250
151	291_R_None	R non	48
152	241_R_VentralAttn	R VeA	32
153	276_R_FrontoParietal	R FrP	48
154	45_L_SMhand	L SMh	127
155	232_R_Auditory	R Aud	36

Index	ROI name	Network	Number of grayordinates
156	117_L_Default	L Def	144
157	172_R_None	R non	98
158	9_L_FrontoParietal	L FrP	49
159	121_L_None	L non	49
160	268_R_Auditory	R Aud	58
161	231_R_VentralAttn	R VeA	96
162	CEREBELLUM_RIGHT	Subct	9144
163	24_L_FrontoParietal	L FrP	111
164	140_L_Visual	L Vis	143
165	72_L_CinguloOperc	L CiO	179
166	132_L_Visual	L Vis	63
167	305_R_None	R non	33
168	235_R_CinguloOperc	R CiO	163
169	265_R_Visual	R Vis	376
170	319_R_FrontoParietal	R FrP	89
171	272_R_FrontoParietal	R FrP	99
172	DIENCEPHALON_VENTRAL_LEFT	Subct	706
173	328_R_FrontoParietal	R FrP	77
174	327_R_FrontoParietal	R FrP	171
175	98_L_Visual	L Vis	84
176	293_R_Visual	R Vis	32
177	207_R_SMhand	R SMh	85
178	168_R_FrontoParietal	R FrP	70
179	288_R_None	R non	22
180	118_L_None	L non	47
181	228_R_VentralAttn	R VeA	56
182	THALAMUS_RIGHT	Subct	1248
183	31_L_SMhand	L SMh	153
184	104_L_Auditory	L Aud	136
185	183_R_Salience	R Sal	40
186	49_L_DorsalAttn	L DoA	60
187	259_R_Default	R Def	350
188	47_L_SMhand	L SMh	183
189	56_L_SMhand	L SMh	240
190	278_R_Default	R Def	74
191	19_L_None	L non	35
192	53_L_SMmouth	L SMm	405
193	84_L_CinguloOperc	L CiO	244
194	13_L_RetrosplenialTemporal	L ReT	134

Index	ROI name	Network	Number of grayordinates
195	279_R_Default	R Def	155
196	177_R_Visual	R Vis	86
197	129_L_None	L non	161
198	52_L_DorsalAttn	L DoA	160
199	196_R_CinguloOperc	R CiO	126
200	209_R_SMhand	R SMh	80
201	245_R_CinguloOperc	R CiO	65
202	229_R_VentralAttn	R VeA	109
203	11_L_None	L non	52
204	249_R_CinguloOperc	R CiO	207
205	66_L_Auditory	L Aud	155
206	76_L_CinguloOperc	L CiO	224
207	145_L_Default	L Def	97
208	330_R_Auditory	R Aud	142
209	257_R_Default	R Def	39
210	82_L_CinguloOperc	L CiO	35
211	33_L_SMhand	L SMh	30
212	289_R_None	R non	34
213	273_R_FrontoParietal	R FrP	167
214	213_R_SMhand	R SMh	281
215	312_R_None	R non	83
216	135_L_None	L non	73
217	326_R_Default	R Def	46
218	22_L_CinguloOperc	L CiO	306
219	299_R_Visual	R Vis	152
220	252_R_DorsalAttn	R DoA	243
221	143_L_RetrosplenialTemporal	L ReT	51
222	26_L_Default	L Def	43
223	263_R_Visual	R Vis	526
224	77_L_Auditory	L Aud	112
225	3_L_SMmouth	L SMm	170
226	302_R_None	R non	34
227	204_R_SMhand	R SMh	35
228	PUTAMEN_LEFT	Subct	1060
229	169_R_Visual	R Vis	38
230	125_L_None	L non	31
231	163_R_SMhand	R SMh	304
232	57_L_SMhand	L SMh	104
233	34_L_CinguloOperc	L CiO	137

Index	ROI name	Network	Number of grayordinates
234	264_R_Visual	R Vis	235
235	179_R_None	R non	45
236	269_R_Auditory	R Aud	84
237	190_R_SMhand	R SMh	196
238	AMYGDALA_RIGHT	Subct	332
239	100_L_DorsalAttn	L DoA	538
240	244_R_Auditory	R Aud	39
241	67_L_Auditory	L Aud	59
242	253_R_DorsalAttn	R DoA	138
243	151_L_Default	L Def	47
244	186_R_Default	R Def	30
245	260_R_FrontoParietal	R FrP	52
246	313_R_RetrosplenialTemporal	R ReT	34
247	102_L_Auditory	L Aud	61
248	166_R_Visual	R Vis	239
249	167_R_FrontoParietal	R FrP	143
250	59_L_SMmouth	L SMm	46
251	40_L_CinguloOperc	L CiO	45
252	29_L_Salience	L Sal	38
253	28_L_CinguloOperc	L CiO	31
254	116_L_Default	L Def	183
255	97_L_Visual	L Vis	255
256	178_R_None	R non	57
257	202_R_SMhand	R SMh	72
258	36_L_SMhand	L SMh	188
259	227_R_Auditory	R Aud	143
260	187_R_CinguloOperc	R CiO	45
261	323_R_Default	R Def	34
262	99_L_Visual	L Vis	244
263	68_L_Auditory	L Aud	76
264	148_L_FrontoParietal	L FrP	68
265	197_R_SMmouth	R SMm	105
266	85_L_VentralAttn	L VeA	54
267	271_R_DorsalAttn	R DoA	115
268	188_R_CinguloOperc	R CiO	66
269	CAUDATE_LEFT	Subct	728
270	41_L_DorsalAttn	L DoA	168
271	203_R_DorsalAttn	R DoA	128
272	133_L_None	L non	70

Index	ROI name	Network	Number of grayordinates
273	321_R_Default	R Def	113
274	124_L_None	L non	34
275	126_L_Default	L Def	51
276	195_R_SMhand	R SMh	73
277	CAUDATE_RIGHT	Subct	755
278	38_L_SMhand	L SMh	243
279	282_R_None	R non	52
280	134_L_None	L non	41
281	216_R_SMhand	R SMh	270
282	310_R_Visual	R Vis	59
283	86_L_VentralAttn	L VeA	56
284	246_R_CinguloOperc	R CiO	60
285	6_L_Default	L Def	887
286	261_R_FrontoParietal	R FrP	37
287	137_L_Visual	L Vis	181
288	284_R_None	R non	79
289	171_R_Auditory	R Aud	129
290	46_L_SMhand	L SMh	52
291	208_R_DorsalAttn	R DoA	69
292	141_L_Visual	L Vis	303
293	215_R_SMhand	R SMh	42
294	88_L_DorsalAttn	L DoA	139
295	192_R_CinguloOperc	R CiO	69
296	55_L_DorsalAttn	L DoA	120
297	193_R_SMhand	R SMh	111
298	5_L_Visual	L Vis	389
299	94_L_Default	L Def	247
300	152_L_Default	L Def	72
301	48_L_SMhand	L SMh	72
302	ACCUMBENS_RIGHT	Subct	140
303	218_R_SMmouth	R SMm	54
304	27_L_CinguloOperc	L CiO	138
305	304_R_None	R non	79
306	20_L_Visual	L Vis	71
307	87_L_DorsalAttn	L DoA	315
308	251_R_Visual	R Vis	179
309	131_L_Visual	L Vis	117
310	65_L_Auditory	L Aud	41
311	175_R_Visual	R Vis	665

Index	ROI name	Network	Number of grayordinates
312	256_R_Visual	R Vis	31
313	69_L_Auditory	L Aud	59
314	15_L_Visual	L Vis	636
315	248_R_CinguloOperc	R CiO	42
316	233_R_Auditory	R Aud	117
317	294_R_RetrosplenialTemporal	R ReT	36
318	250_R_DorsalAttn	R DoA	38
319	70_L_Auditory	L Aud	33
320	191_R_SMhand	R SMh	256
321	8_L_Visual	L Vis	177
322	301_R_None	R non	68
323	130_L_RetrosplenialTemporal	L ReT	145
324	298_R_Visual	R Vis	407
325	176_R_Visual	R Vis	139
326	115_L_None	L non	34
327	307_R_Visual	R Vis	100
328	285_R_None	R non	14
329	149_L_FrontoParietal	L FrP	48
330	224_R_Auditory	R Aud	135
331	300_R_None	R non	73
332	255_R_Visual	R Vis	67
333	226_R_VentralAttn	R VeA	55
334	120_L_None	L non	108
335	32_L_SMhand	L SMh	58
336	309_R_Visual	R Vis	66
337	10_L_Auditory	L Aud	106
338	42_L_DorsalAttn	L DoA	48
339	211_R_DorsalAttn	R DoA	181
340	161_L_VentralAttn	L VeA	37
341	306_R_None	R non	52
342	210_R_SMhand	R SMh	35
343	58_L_SMhand	L SMh	119
344	189_R_DorsalAttn	R DoA	258
345	329_R_Auditory	R Aud	10
346	16_L_Visual	L Vis	39
347	303_R_None	R non	70
348	95_L_DorsalAttn	L DoA	45
349	35_L_SMhand	L SMh	134
350	308_R_Visual	R Vis	84

Index	ROI name	Network	Number of grayordinates
351	237_R_VentralAttn	R VeA	60
352	17_L_Visual	L Vis	14

Table S3. Mapping of the top 11 unclassified ROIs from Gordon into Yeo, based on grayordinates. The grayordinates from each ROI were map into each one of the 7 networks proposed by Yeo

Relative importance	Gordon ROI name	# grayordinates in Gordon	Yeo-Limbic	Yeo-FrP	Yeo-Def	Yeo-No assignment	Winner take all
4	144_L_None	74	8	0	**35**	31	Def
20	281_R_None	76	0	13	**63**	0	Def
21	122_L_None	57	**57**	0	0	0	Limbic
23	119_L_None	42	0	15	**27**	0	Def
29	18_L_None	62	0	0	1	**61**	Non
43	296_R_None	77	**46**	0	24	7	Limbic
67	283_R_None	106	**85**	21	0	0	Limbic
80	123_L_None	82	**82**	0	0	0	Limbic
84	297_R_None	44	**44**	0	0	0	Limbic
95	142_L_None	71	**52**	0	1	18	Limbic
98	128_L_None	137	**80**	0	57	0	Limbic

Table S4. Sibling status for participants form the Human Connectome Project[1].

# families	Descendants per family	Sibling type			Total
		Identical twins	Non identical twins	Siblings no twins	
70	1	0	0	0	**0**
49	2	5	10	34	**49**
10	3	5	1	24	**30**
Total		**10**	**11**	**58**	**79**

[1] Open access and restricted data from the Washington University in Saint Louis-University of Minnesota (WU-Minn) HCP consortium "500 Subjects release" (June 2014) was generously provided after registration and agreement of the Open Access Data Use Terms and Restricted Data Use Terms

Table S5. Partitions used for classifying siblings from unrelated populations using HCP data and SVM.

Method	Identical twins		Non-identical twins		Siblings-no-twins		Unrelated	
	In-sample	Out-of-sample	In-sample	Out-of-sample	In-sample	Out-of-sample	In-sample	Out-of-sample
Connectotyping	16	4	18	4	104	12	138	20
Correlations of connectivity matrices	6	4	7	4	54	4	67	12

Supplemental References.

Benjamini, Y., & Hochberg, Y. (1995). Controlling the False Discovery Rate: a Practical and Powerful Approach to Multiple Testing. *J.R. Statist, Soc, B*, *57*(1), 289–300.

Dale, A.M., Fischl, B. & Sereno, M.I., 1999. Cortical surface-based analysis. I. Segmentation and surface reconstruction. *NeuroImage*, 9(2), pp.179–94.

Desikan, R.S. et al., 2006. An automated labeling system for subdividing the human cerebral cortex on MRI scans into gyral based regions of interest. *NeuroImage*, 31(3), pp.968–80.

Dosenbach, N.U.F. et al., 2010. Prediction of individual brain maturity using fMRI. *Science (New York, N.Y.)*, 329(5997), pp.1358–61.

Fischl, B. & Dale, A.M., 2000. Measuring the thickness of the human cerebral cortex from magnetic resonance images. *Proceedings of the National Academy of Sciences of the United States of America*, 97(20), pp.11050–5.

Glahn, D. C., Winkler, a M., Kochunov, P., Almasy, L., Duggirala, R., Carless, M. a, … Blangero, J. (2010). Genetic control over the resting brain. *Proceedings of the National Academy of Sciences of the United States of America*, *107*(3), 1223–1228. http://doi.org/10.1073/pnas.0909969107

Greve, D.N. & Fischl, B., 2009. Accurate and robust brain image alignment using boundary-based registration. *NeuroImage*, 48(1), pp.63–72.

Jenkinson, M. et al., 2012. FSL. *NeuroImage*, 62(2), pp.782–90.

Smith, S.M. et al., 2004. Advances in functional and structural MR image analysis and implementation as FSL. *NeuroImage*, 23 Suppl 1, pp.S208–19.

Visscher, P. M., & Goddard, M. E. (2015). A General Unified Framework to Assess the Sampling Variance of Heritability Estimates Using Pedigree or Marker-based Relationships. *Genetics*, *199*(January), 223–232.

Woolrich, M.W. et al., 2009. Bayesian analysis of neuroimaging data in FSL. *NeuroImage*, 45(1 Suppl), pp.S173–86.